

# Propellant Injection in a Liquid Oxygen/Gaseous Hydrogen Rocket Engine

Wolfgang Mayer\*

*DLR, German Aerospace Research Establishment, Lampoldshausen, 74239 Hardthausen, Germany*  
and

Hiroshi Tamura†

*National Aerospace Laboratory, Miyagi 981-15, Japan*

Flow visualizations and measurements related to the propellant injection, mixing, evaporation, and combustion in a liquid rocket engine combustor at supercritical chamber pressures are presented. An experimental motor consisting of a single coaxial shear injector element and a cylindrical chamber with optical access has been developed. Flow visualizations and measurements of injection, spray formation, and supercritical mixing for liquid oxygen (LOX)/gaseous hydrogen propellants at chamber pressures up to 10.0 MPa are presented. The injection visualizations and studies under combusting conditions revealed a remarkable difference between subcritical spray formation and evaporation, and the supercritical injection and mixing processes. The study shows that approaching supercritical chamber pressures, injection can no longer be regarded as an atomization or spray formation process. Under these conditions droplets no longer exist. The visualizations revealed that at chamber pressures equal to or higher than 4.5 MPa, oxygen forms thread- or stringy-like structures, which rapidly dissolve. The role of injector tip design and LOX post recess are studied. The flame is attached to the LOX post and develops in the LOX post wake. It seems that the flame tends to separate the propellants. The measurement of the flame radiation spectra revealed a peak in the uv and a large amount of radiation in the visible range.

## Introduction

WITH increasing development costs for future or improved rocket engines, the need for eliminating a large part of the trial-and-error phase of development becomes more urgent. Very decisive and critical components of a rocket engine are the injector head and combustion chamber, but the basic concepts of injection and combustion of propellants are not well understood.

Coaxial shear injectors have proven to be advantageous for the injection of propellants in liquid rocket engines used, e.g., in the ARIANE 5 central stage motor HM60, the Space Shuttle Main Engine, the LE 7 engine, and others. Typically, the oxygen leaves the injector in the form of a turbulent freejet with a diameter of a few millimeters and an exit velocity of about 30 m/s. The atomizing hydrogen enters the combustion chamber with an approximately 10 times higher velocity through an annular port with a height of approximately 1 mm. Propellant temperatures are around 100 K. The combustion chamber pressure is on the order of 10 MPa. Both propellants are injected under supercritical pressure and temperature conditions, except that the injection temperature of oxygen is subcritical. The critical pressures of oxygen and hydrogen are 5.09 and 1.31 MPa, and the critical temperatures are 154.8 and 33.2 K, respectively. As the injection is a nonequilibrium process, propellant interphase phenomena cannot be easily predicted or characterized using equilibrium thermodynamics.

It is recognized that much refined work has been done concerning the break-up and atomization of liquid jets without combustion. In the case of coaxial shear atomization at subcritical conditions, the basic cold flow break-up mechanisms are now understood to a certain degree.<sup>1,2</sup> Puissant et al.<sup>3</sup> report on first experimental studies of shear coaxial injection using liquid and gaseous nitrogen as simulants at supercritical pressure conditions. Recently, Schik et al.<sup>4</sup> published related work on injection under supercritical noncombusting conditions using liquid nitrogen and helium.

However, the interrelation between the fluid dynamic processes such as atomization, mixing, and recirculation on the one hand, and the physicochemical processes of evaporation and combustion on the other hand, is still far from being understood to a satisfactory degree.

About 35 years ago, the first successful attempts were undertaken to visualize and measure combustion phenomena inside a firing combustion chamber.<sup>5</sup> Recently, attempts to characterize the near-injector region in a unielement coaxial injector rocket chamber at pressures up to 3.1 MPa have been reported by Beisler et al.<sup>6</sup> At DLR Lampoldshausen, a small model combustor with optical access has been used for injection studies. A chamber designed for pressures up to 2.0 MPa was used to collect basic impressions on the influence of combustion on the injection process. Evaluation of the photographic material indicates a strong influence of fluid mechanics on the combustion process.<sup>7,8</sup> Small droplets at the outer spray boundary are rapidly vaporized.

Little or no information is available with respect to the formation of propellant sprays, their evaporation, and subsequent combustion under actual rocket chamber conditions. This is particularly true for the case of high pressure and supercritical combustion.

The objective of this research is to gain a realistic insight into the injection and combustion processes in liquid oxygen/gaseous hydrogen (LOX/GH<sub>2</sub>) rocket engine combustors by observing directly the propellants' injection, oxygen ligament formation, and subsequent evaporation and combustion under

Presented as Paper 95-2433 at the AIAA/ASME/SAE/ASEE 31st Joint Propulsion Conference and Exhibit, San Diego, CA, July 10–12, 1995; received July 14, 1995; revision received Nov. 22, 1995; accepted for publication Dec. 12, 1995. Copyright © by W. Mayer and H. Tamura. Published by the American Institute of Aeronautics and Astronautics, Inc., with permission.

\*Research Engineer, Head Propellant Injection Research Group, Member AIAA.

†Research Engineer, Kakuda Research Center, Head Rocket Combustor Laboratory, Member AIAA.

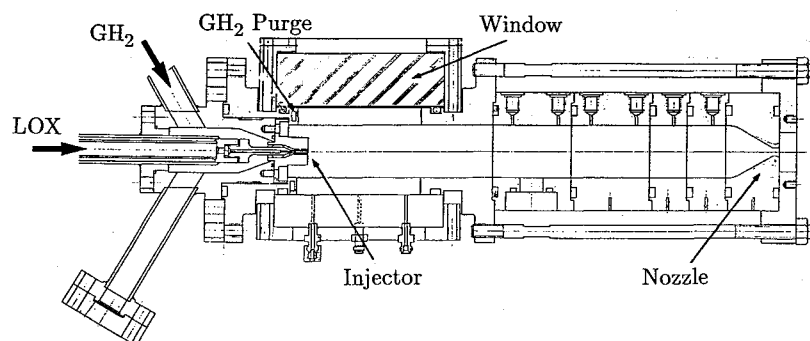


Fig. 1 Experimental rocket motor. Combustion chamber length and chamber diameter are 400 and 40 mm, respectively.

actual operating conditions at chamber pressures up to 10.0 MPa.

For this purpose, an experimental rocket motor with optical access has been used, and injection and mixing have been studied under cold flow and combusting conditions using flow visualization techniques.

### Test Facility and Experimental Setup

An experimental rocket motor with two flat windows in opposite walls has been developed as sketched in Fig. 1. It consists of an injector head with a single shear coaxial element, a circular, uncooled combustion chamber with a length and diameter of 400 and 40 mm, respectively, and a variable (exchangeable) nozzle. The window section was cooled by a layer of gaseous hydrogen. The purge flow was injected parallel to the windows in the direction of the nozzle. Metal dummy windows with thermocouples have been used to develop the startup and shutdown sequence and a suitable window cooling technique (also shown in Fig. 1).

A nontapered shear coaxial injector with and without recess was evaluated with exchangeable injector faceplates of different fuel annulus diameters. It was possible to make experiments at constant propellant mixture ratio and injection velocities (i.e., constant velocity ratio), even at different chamber pressures. The injector LOX postbaseline dimensions were an i.d. of 1 mm with a wall thickness of 0.3 mm. Maximum injector flow rates in this configuration at a determined mixture ratio of  $O/F = 5$  were 40 and 8 g/s for oxidizer and fuel, respectively. LOX was supplied to the test section from a helium-pressurized vacuum jacketed 70-m<sup>3</sup> storage tank. The supply of GH<sub>2</sub> to the injector and window purge ports was from a 20.0-MPa bottle depot. Flow rates were measured using turbine flow meters. To cool down the cryogenic supply line a liquid nitrogen cooling jacket was installed onto this line between the LOX tank and LOX dome. Chilledown of the LOX line made it possible to reach steady-state firing conditions in less than 1 s. Ignition was done by a small gaseous oxygen/hydrogen pilot flame. The igniter was mounted on the lower part of the chamber wall. Typical time duration of a firing was 5 s, including start-up transients of approximately 0.1 s.

### Flow Visualization Technique

Several different visualization techniques were used that are stated in the respective sections.

At low chamber pressures (2.0 MPa or less), flow visualization studies were done with a standard camera and a flash-light in a shadowgraph and schlieren setup. Typical shutter time was 1/60 s. A spark flashlight (Fischer NANOLITE, High Speed Photo Systeme GmbH) was used that has a typical pulse duration of less than 50 ns. The optical setup and filters have been carefully selected and tested to determine the optimum between fadeout of reacting propellant radiation and flashlight intensity losses.

At higher chamber pressures the radiance of the flame increases dramatically. It has to be emphasized that we attempted

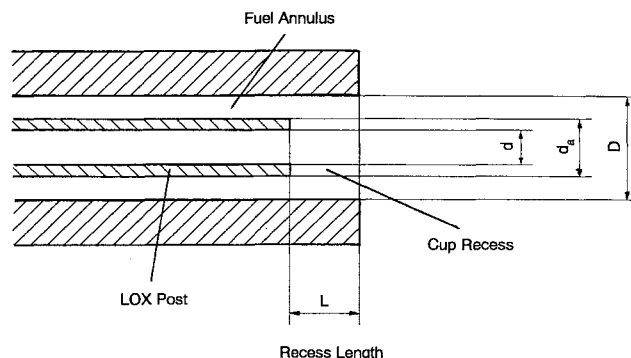


Fig. 2 Coaxial injector.

to observe a flow process under severe conditions: flow velocities up to 300 m/s, high chamber pressure, fluid temperatures ranging from 100 K up to 3600 K, and strong radiation of flame. It revealed, as expected, that the applicability of flow visualization or measurement techniques using standard optical or laser-optical methods is limited. Therefore, a special optical setup based upon shadowgraphy, including a high-speed rotating disc shutter, has been developed. The shutter speed was less than 1/1000 s. To fade out radiance of the flame, an aperture was set between the combustion chamber and camera lenses. The light of the flash lamp was focused down to the lenses aperture and is, therefore, not parallel. That is why the density gradients are also visible when using this technique.

High-speed video motion analysis (Kodak Motion Analyser) of the flow and the flame has been done. The spectrum and intensity of the flame has been measured using a spectrometer (MCPD 2000, IMUC-7000, Otsuka Electronics).

### Firing Test Conditions

The baseline dimensions of the injector (see Fig. 2) and the chosen firing test conditions covered in this study were as follows:

LOX post i.d. $d$ :	1 mm
LOX post o.d. $d_a$ :	1.6 mm
Fuel annulus diameter $D$ :	2.5–3.9 mm
Recess length $L$ :	0–2.9 mm
Chamber pressure:	1.0–10.0 MPa
Oxygen injection velocity:	10–30 m/s
Oxygen injection temperature:	100 K
Hydrogen injection velocity:	200–300 m/s
Hydrogen injection temperature:	150–300 K
Mixture ratio $O/F$ :	2–5
$c^*$ efficiency:	0.88–0.97

Numbers represent average values of test data. A number range indicates that the parameter was varied to study its influence on mixing and combustion.

Reference cases are firing tests with a nonrecessed injector at 1.5-, 4.5-, 6.0-, and 10.0-MPa chamber pressure ( $p_c$ , test cases 1–4, see Table 1). The corresponding oxygen and hydrogen velocities ( $u_{\text{LOX}}$ ,  $u_{\text{GH}_2}$ ) were 30 and 300 m/s, respectively, except for the 1.5-MPa case (test case 1), where LOX velocity was reduced to 10 m/s. This velocity reduction was necessary because the mixing efficiency at 1.5-MPa chamber pressure is so low that otherwise a large part of the LOX jet and ligaments would leave the chamber unburned and could not be visualized. Unless otherwise stated, LOX temperature  $T_{\text{LOX}}$  was 100 K, and hydrogen temperature  $T_{\text{GH}_2}$  was 300 K. Injector dimensions for the reference cases (test cases 1–4) were as follows:  $d = 1$  mm,  $d_a = 1.6$  mm, and  $D = 3.9$  mm. The final parallel part of the injector had a length of 20 mm. Nozzle throat diameter was 5.8 mm.

Figure 3 shows the windowed rocket motor during operation.

Table 1 Test case conditions

Test case	$p_c$ , MPa	$u_{\text{LOX}}$ , m/s	$u_{\text{GH}_2}$ , m/s	$T_{\text{LOX}}$ , K	$T_{\text{GH}_2}$ , K
1	1.5	10	300	100	300
2	4.5	30	300	100	300
3	6.0	30	300	100	300
4	10.0	30	300	100	300

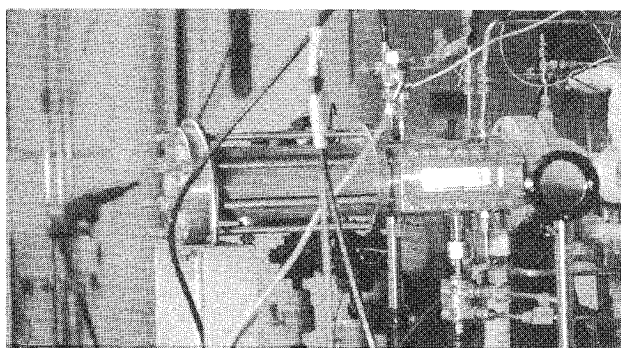


Fig. 3 Rocket motor during operation.

## Oxygen Jet Visualizations

The following figures are arranged in the order of increasing chamber pressure (1.5, 6.0, and 10.0 MPa, test case 1, 3, and 4, respectively), and demonstrate the effect of chamber pressure to the atomization and mixing process.

### Low Chamber Pressures

Figure 4 shows the photographs of the 1.5-MPa condition (test case 1) taken with a standard shadowgraph setup. At chamber pressures much less than the critical pressure of oxygen ( $<5.09$  MPa), the LOX jet is atomized forming a spray comparable to the flow pattern of cold flow atomization before ignition, or as known from cold flow studies (see e.g., Ref. 1). Ligaments are detached from the LOX jet surface, which form round droplets and finally evaporate. At the 1.5-MPa chamber pressure experiments, secondary break up (droplet vibrational- and bag-type break up) could be observed. Because of the rapid vaporization of the droplets in a burning spray, the droplet number density is rather low compared to the cold flow case. Most of the droplets are nonspherical. Note also the very smooth surface of the LOX jet close to the injector.

### High and Supercritical Chamber Pressures

The used visualization technique was on principal shadowgraphy. To fade out the strong radiation of the burning propellants, the light of the flash lamp (pulse duration less than 50 ns) was focused down to the lenses aperture. A second aperture was set between the combustion chamber and camera lenses. Therefore, density gradients are also visible. Since the hydrogen is coannular, and as we will see later, the flame surrounds the LOX jet, one must realize that any visualization of the LOX structure inside must occur through all of these layers. The interpretation of the photographs has to be done very carefully using preferably original prints or high-quality copies.

Upon approaching and exceeding supercritical pressure, droplets no longer exist (Figs. 5 and 6, test cases 3 and 4, respectively). From the LOX jet core, schlieren- (stringy-) or thread-like structures develop and grow, which do not detach, but rapidly dissolve and fade away. Several tens of jet diameters further downstream the LOX core break up into large

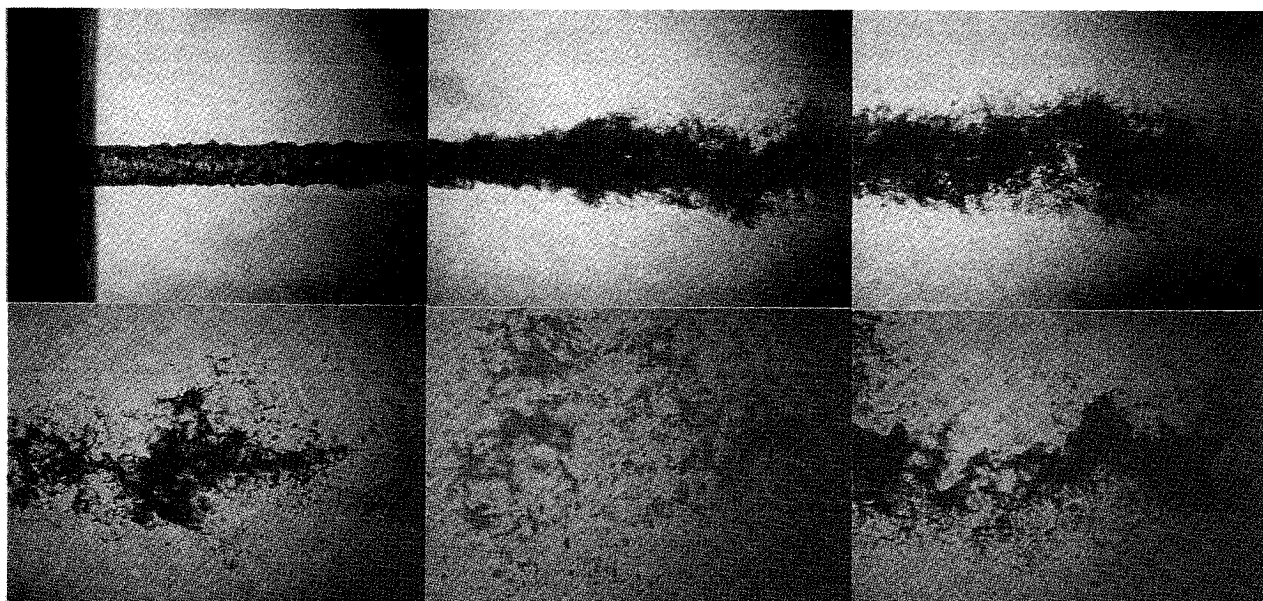


Fig. 4 Oxygen jet, subcritical injection, combusting condition: oxygen velocity is 10 m/s, hydrogen velocity is 300 m/s,  $d = 1$  mm, chamber pressure 1.5 MPa (test case 1), from left to right and top to bottom: axial position  $x = 0$  (faceplate), 12, 24, 36, 48, and 60 mm.

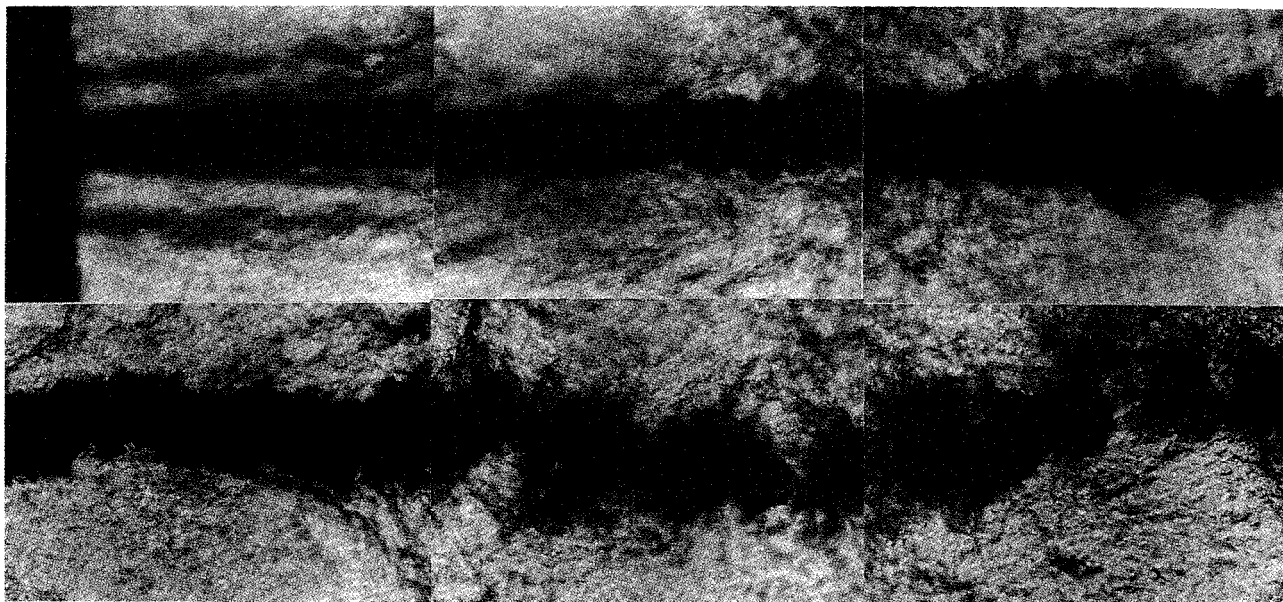


Fig. 5 Oxygen jet, supercritical injection, combusting condition: oxygen velocity is 30 m/s, hydrogen velocity is 300 m/s,  $d = 1$  mm, chamber pressure 6.0 MPa (test case 3), from left to right and top to bottom: axial position  $x = 0$  (faceplate), 12, 24, 36, 48, and 60 mm.

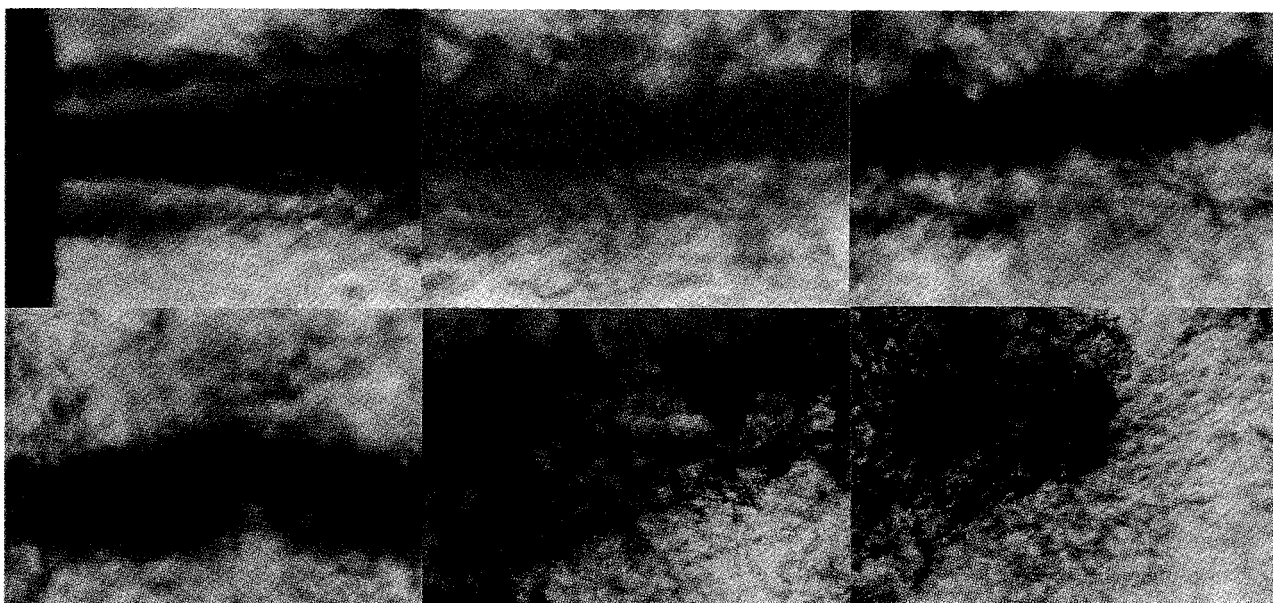


Fig. 6 Burning oxygen jet, supercritical injection, combusting condition: oxygen velocity is 30 m/s, hydrogen velocity is 300 m/s,  $d = 1$  mm, chamber pressure 10.0 MPa (test case 4), from left to right and top to bottom: axial position  $x = 0$  (faceplate), 12, 24, 36, 48, and 60 mm.

LOX lumps, which dissolve in the same manner. The jet break-up length (average length of connected LOX) decreases with increasing chamber pressure. In the 4.5- (test case 2) and 6.0-MPa cases (test case 3, Fig. 5), mixing and combustion are not complete at the end of the visualized area. The 10.0-MPa case (test case 4, last photographs of Fig. 6), however, shows that the break-up length and the end of the oxygen jet (position  $x = 60$  mm), i.e., the location where the oxygen is fully depleted, are almost the same. During several tests not a single oxygen lump could be visualized downstream of position  $x = 70$  mm. The end of the oxygen jet coincides with the vanishing flame, i.e., uv radiation (see the upcoming Structure of Flame section).

The macroscopic behavior of the oxygen jet, which is already indicated in Figs. 4–6, is demonstrated in Fig. 7 for the

4.5-MPa case (test case 2). The photographs have been taken at a repetition rate of 12,000 frames/s using a Kodak Motion Analyser and a simple 150-W film lamp in a backlight setup. The visible area reaches from the faceplate up to 70 mm downstream. The first six of the photographs (frames 235–240) show the time transient behavior of the oxygen jet during startup transients. Typical time duration of startup transients was 0.1 s. For these frames, although ignition has already taken place, several pulsations of the oxygen jet were observed. During steady-state combustion (Fig. 7, frames 704–706), nonaxisymmetric, snake-like oscillations of the jet with an amplitude of a few jet diameters can be seen. The high-speed photograph sequences revealed a further important phenomenon: the oxygen jet is accelerated and nearly doubles its velocity from the faceplate to 70 mm downstream.

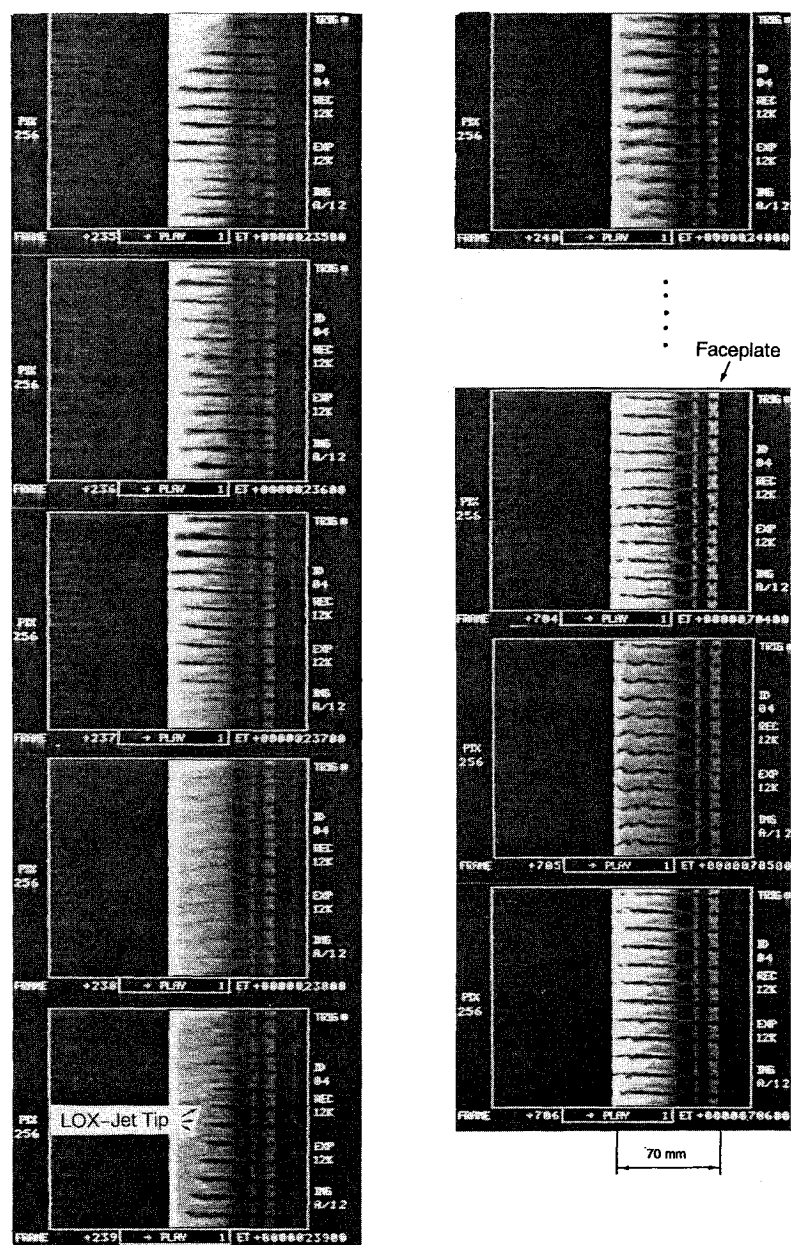


Fig. 7 High-speed sequence: startup transients and steady-state combustion, chamber pressure 4.5 MPa (test case 2), oxygen and hydrogen injection velocities are 30 and 300 m/s, respectively, 12,000 frames/s.

### Near Injector Region

#### Principal Character of Flow

A very important observation of this study is the coincidence of LOX post wake and flame and its interaction with the fuel/oxygen shear layer (Figs. 8 and 9). The photographs in Figs. 8 and 9 are taken at the same firing test conditions (4.5 MPa, test case 2); however, two different visualization techniques have been used. This has been done on the one hand to discover the location of the flame (top photographs of Figs. 8 and 9), and on the other hand to visualize the corresponding flow-field (bottom photographs of Figs. 8 and 9). The used visualization technique was on principal shadowgraphy. For the flame visualizations a standard shadowgraph setup was used (top photographs of Figs. 8 and 9). For the flow visualizations to fade out the radiation of the burning propellants, the light of the flash lamp (pulse duration less than 50 ns) was once again focused down to the lenses aperture and is therefore not parallel (bottom photographs of Figs. 8 and 9). That is why density gradients are also visible.

The flame always attaches instantaneously after ignition to the LOX post. As indicated by the bright flame spot close to the LOX post tip, it seems that the strong recirculation zone behind the LOX post acts as a flameholder. This could be observed in the entire range of the tested conditions in this study for injectors with and without recess, and for an LOX post tip thickness of only 0.3 mm. In the small, but intensive, recirculation zone behind the LOX post, a well-mixed flame with strong radiation forms. The influence of this LOX post wake, which can be tracked at least 15 LOX jet diameters downstream, significantly controls the LOX/GH<sub>2</sub> mixing process; the interface between the propellants LOX and hydrogen is separated by a layer of reacting combustion gases. Further downstream, the divergent flame increases in size and radiation intensity, especially in the break-up or heavy mixing zone, where most of the combustion reaction is taking place (see also the upcoming Oxygen Jet Break-Up Region and Structure of Flame sections).

#### Effects at Low Chamber Pressures

Figure 10 demonstrates the effect of the flame on the LOX



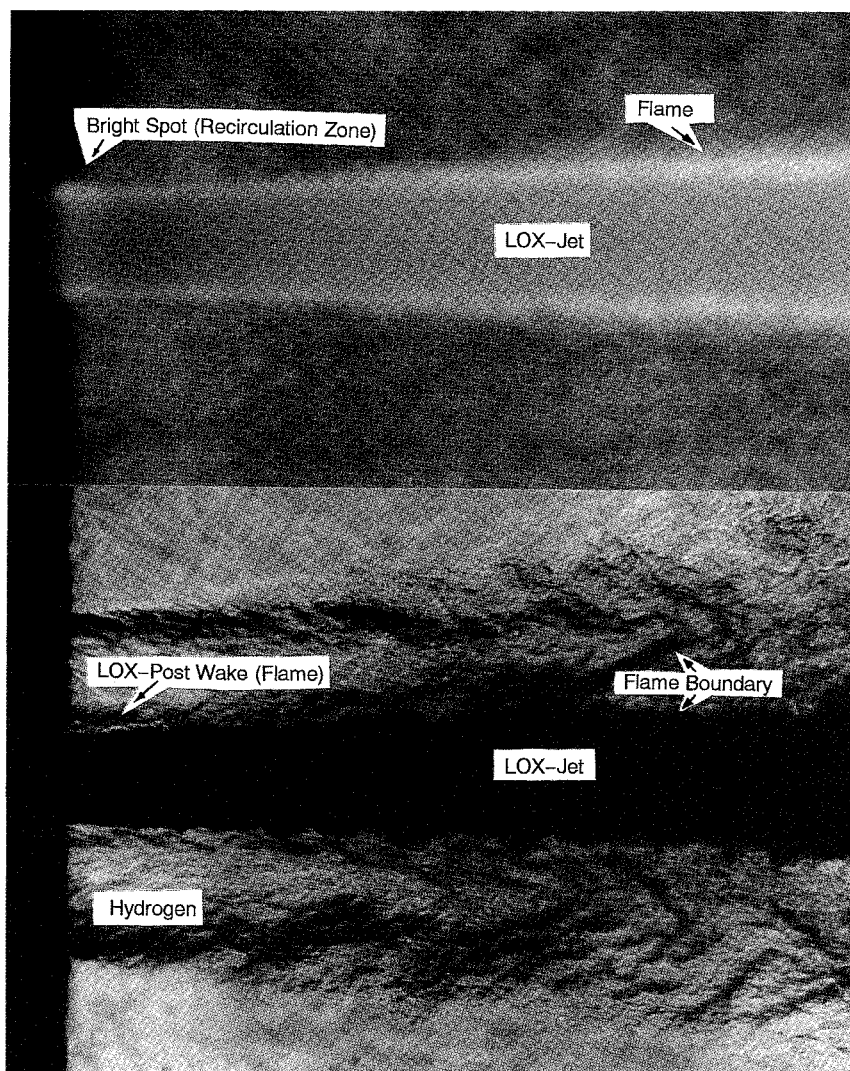


Fig. 8 Near injector region, combustor condition: flame (top) and corresponding flowfield (bottom), oxygen and hydrogen velocities are 30 and 300 m/s, respectively,  $d = 1$  mm, chamber pressure is 4.5 MPa (test case 2).

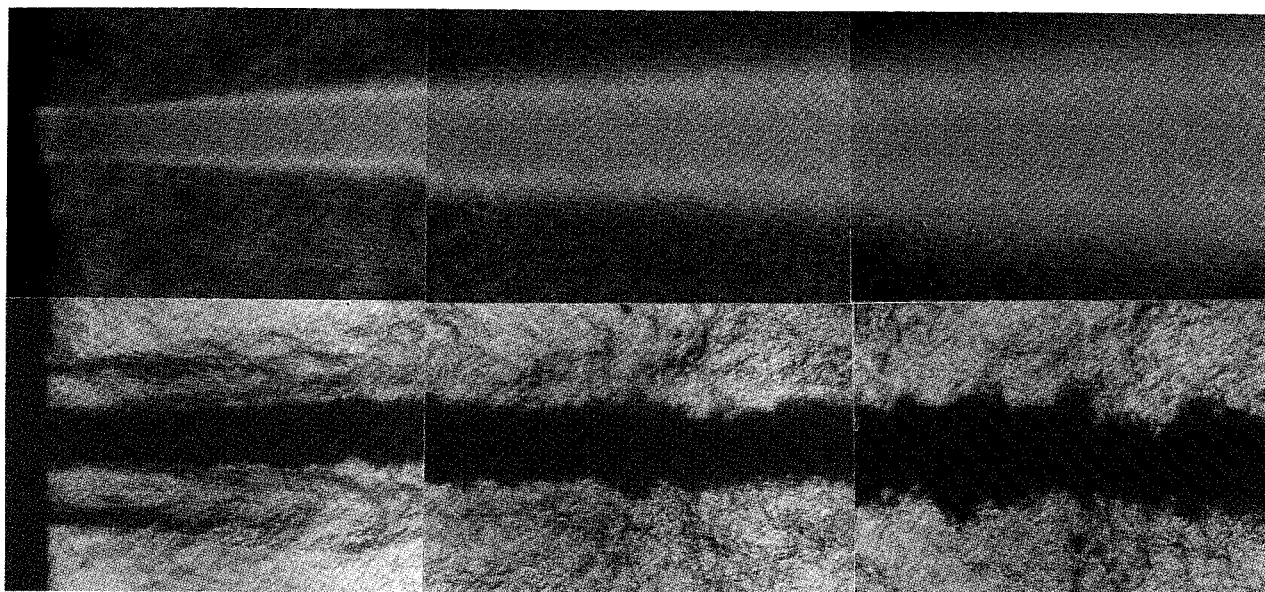


Fig. 9 Combustor condition: flame (top) and corresponding flowfield (bottom), oxygen and hydrogen velocities are 30 and 300 m/s, respectively,  $d = 1$  mm, chamber pressure is 4.5 MPa (test case 2).

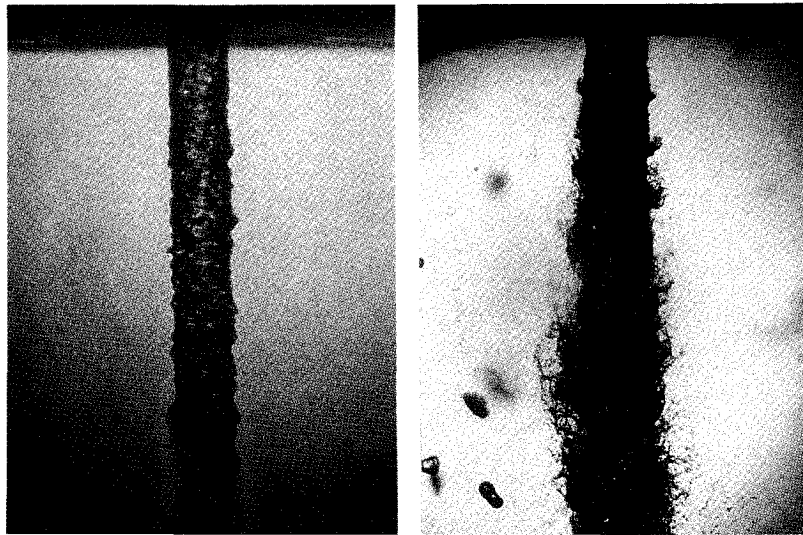


Fig. 10 LOX jet, near injector region, LOX velocity 10 m/s, hydrogen velocity 300 m/s, chamber pressure 1.5 MPa,  $d = 1$  mm; left photograph: burning condition, right photograph: cold flow injection, before ignition.

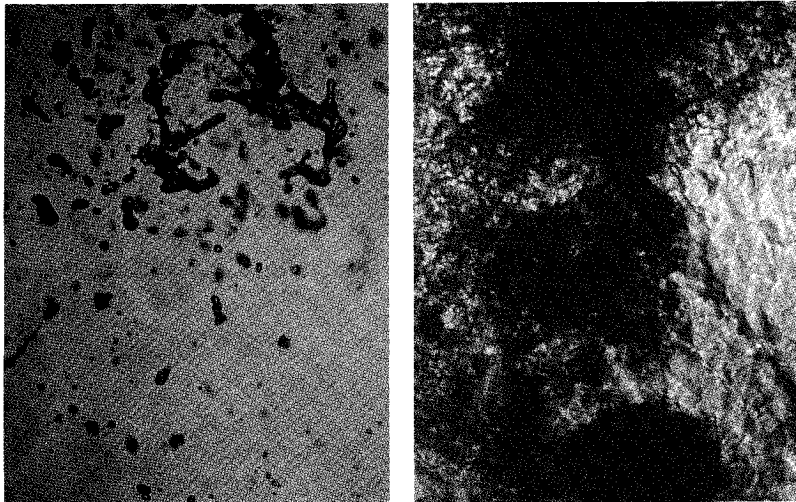


Fig. 11 Burning oxygen, 60 mm downstream of faceplate, main flow direction from top to bottom, visible area size  $6.0 \times 4.8$  mm; chamber pressure of the left and right photographs is 1.5 and 6.0 MPa, respectively.

jet as a comparison of cold flow injection and injection under firing condition. In both cases the chamber pressure is 1.5 MPa (test case 1). In the cold flow case, fine oxidizer threads and droplets are visible. In the combustive case at low chamber pressures, the fine surface structures rapidly vaporize and droplets are never formed. No droplets can be observed in the vicinity of the injector. It is noteworthy that the residual surface tension forms a round liquid jet. The latter effect could not be observed at chamber pressures equal or higher than 4.5 MPa.

#### Oxygen Jet Break-Up Region

Figure 11 (main flow direction from top to bottom) shows magnified photographs of the flowfield at a location in the chamber 60 mm downstream of the injector faceplate for the cases of 1.5- and 6.0-MPa chamber pressure, respectively.

At this position the oxygen jet is already broken up. This area may be characterized as the heavy mixing zone, which includes the maximum amplitudes of oxygen jet oscillations (see also Figs. 4, 5, and 7), slight widening of the oxygen jet and of the flame, dispersion of the oxygen droplets, ligaments or the threads, and strongest combustion radiation. Figure 11 demonstrates once again the remarkable change between sub-

and supercritical pressure conditions. At low chamber pressures, oxygen droplets form and break up as known from cold flow (e.g., water/air) atomization studies. Upon approaching and exceeding supercritical pressures, oxygen develops thread- or stringy-like structures.

#### Propellant Interface Phenomena

The influence of the hydrogen injection temperature on mixing performance in the near injector region has been studied in the range between 150–300 K. Two different chamber pressures were selected for comparison (6.0 and 10.0 MPa). All other test parameters in this experiment, e.g., injector geometry, were kept constant. Oxygen and hydrogen injection velocities were kept constant at 30 and 300 m/s, respectively. Because of the marginal, though not exactly known, value of the surface tension, the Weber number doesn't seem to be appropriate to characterize the propellant interface processes. Assuming a momentum ratio or rather a fuel stagnation pressure dependency of mixing process (the LOX momentum is almost constant in this study), one may expect that decreased hydrogen injection temperature, i.e., increased hydrogen density, will intensify the mixing process. When increasing the chamber

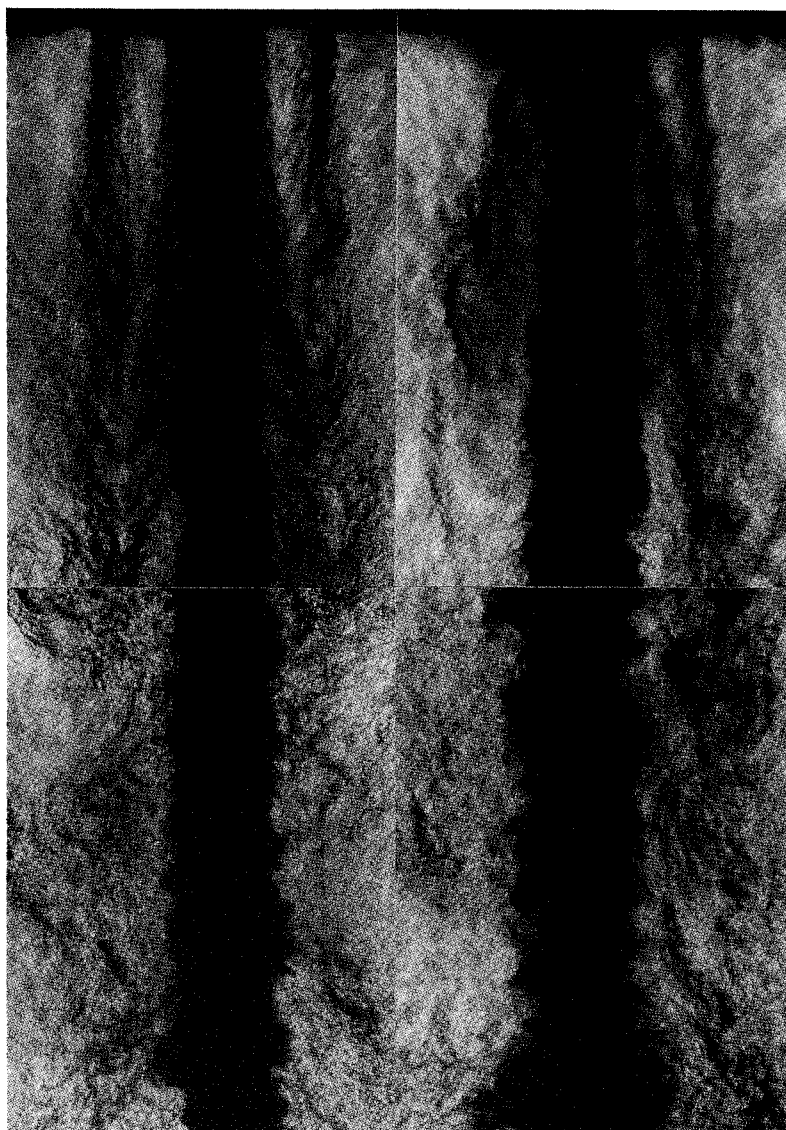


Fig. 12 Comparison of the recessed (right photograph) and the nonrecessed (left photograph) LOX post, chamber pressure is 4.5 MPa.

pressure, one may expect that it will intensify the mixing process likewise.

However, it turned out that a variation of the hydrogen temperature is less effective compared to the effect of absolute chamber pressure. The higher the chamber pressure, the stronger the mixing process. Most relevant for the mixing process in the shear layer between the propellants is the velocity gradient, but also the density of the fluids. The density of the fluids in this layer is influenced by the combustion reaction (temperature) and depends on the ambient chamber pressure. It seems that the flame tends to separate the propellants.

#### Effects of Injector Design on Flowfield

The effect of the injector design has been studied. The influence of LOX post tip wall thickness on the development of the flame is evident (see the Near Injector Region section). A noteworthy result is the comparison of injection with and without recessed LOX post (test case 2). To demonstrate the tendencies, the LOX post was recessed significantly: the recess length was 2.9 mm equivalent to 2.9 LOX post i.d. The fuel annulus diameter was 3.0 mm. Without recess, the propellants enter the combustion chamber as parallel jets that smoothly diverge (see Fig. 12). The LOX jet is straight and the LOX post wake, i.e., the flame zone develops. In the case of the recessed LOX post, the fuel enters the combustion chamber as

a divergent jet. The LOX post wake is more developed and soon reaches the outer boundary of the hydrogen flow. The LOX jet itself seems much more disrupted compared to the nonrecessed case. Further downstream ( $>20$  mm) the difference between recessed and nonrecessed LOX post becomes less and less visible. The known effect of LOX post recess to combustion stability can now be understood in more detail. The results of this study led to the following hypothesis: It is not the improved atomization performance as known from cold flow tests. The far field with and without recess looks the same. Also in regard to performance, recess has no major effect on it. However, it seems that the cup recess region can be regarded as a small and undisturbed combustion chamber, which always keeps the propellants ignited and well mixed in an area close to the injector, insensible to disturbances in the chamber.

#### Structure of Flame

Spectra and relative intensities of the LOX/hydrogen flame have been measured along the oxygen jet axis during startup transients and at steady-state combustion conditions. Typical sampling time of the point measurement was between 5–50 ms. The spectral resolution was between 0.9–1.7 nm.

Figure 13 shows the flame in the visible range during the ignition period and during steady-state combustion conditions.



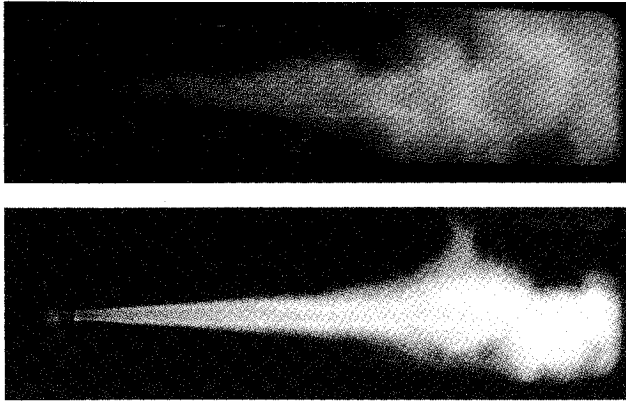


Fig. 13 Flame during ignition (top photograph) and steady-state combustion (bottom photograph), 6.0 MPa, visible range, window size  $80 \times 25$  mm.

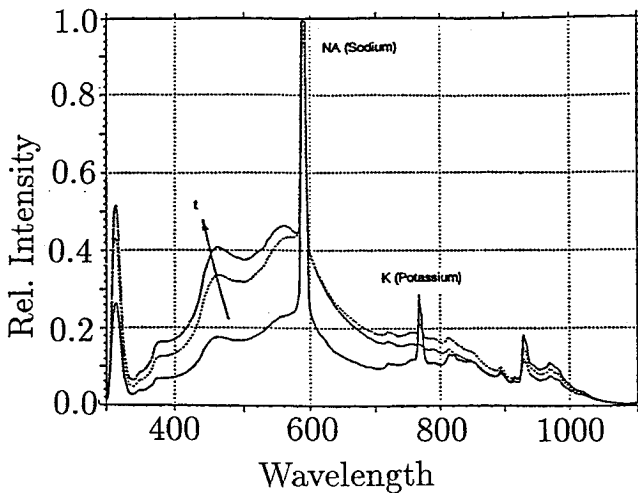


Fig. 14 Spectrum during startup transients, relative intensity, time increment is 0.05 s, 6.0 MPa (test case 3).

During startup, the fuel rich flame shows its typical orangish glow because of the contamination of the hydrogen with sodium. Another dominant peak results from potassium. Both contaminants are a residue of the hydrogen drying process.<sup>9</sup> Shadowgraphy with a low-intensity light source has been used. The green color in the background of Fig. 13 is an artifact of the light source.

Figure 14 shows the corresponding measured spectra at position  $x = 70$  mm downstream from the faceplate (test case 3). Time duration of start-up transients (chamber pressure, mass flow rates, etc.) was 0.1 s. The last curve of Fig. 14 represents almost steady-state conditions. The emissions in the uv wavelength band indicate the reaction and combustion of hydrogen and oxygen (OH emission).

For the case of 6.0-MPa chamber pressure (test case 3, steady-state condition) the full spectra ranging from uv up to infrared has been measured with a resolution of 1.7 nm (Fig. 15). A corresponding flame photograph is presented in Fig. 16. It is remarkable that the radiation intensity downstream ( $x = 70$  mm from the faceplate) is more than 10 times stronger than close to the injector ( $x = 10$  mm). It seems that the largest part of the combustion process is taking place in the heavy mixing zone, as already indicated in the spark photographs (Fig. 5). The spectrum measurements also revealed that a large amount of radiation is in the visible range, probably because of the emission bands of water vapor.

Once again for the 6.0-MPa case, the uv peaks at three different positions are shown in Fig. 17. The spectral resolution was 0.9 nm. The spectrum (wavelength band) is almost the

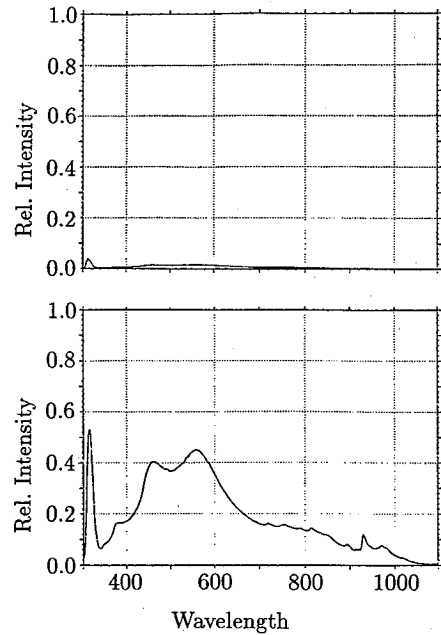


Fig. 15 Spectra of oxygen/hydrogen flame, range 300–1100 nm, 6.0 MPa, test case 3,  $x = 10$  mm (top) and 70 mm (bottom) from faceplate.

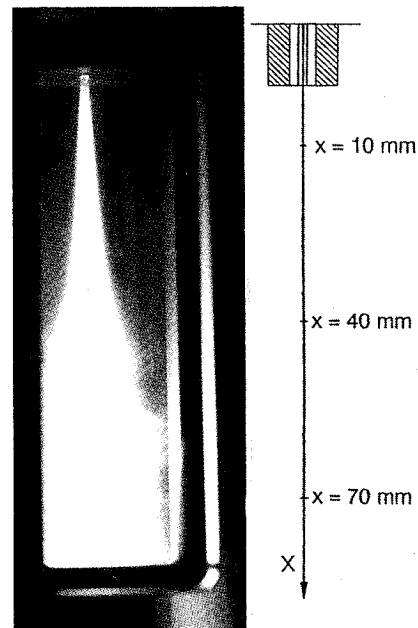


Fig. 16 Flame photograph (window size  $80 \times 25$  mm,  $t = 1/60$  s, 6.0 MPa, test case 3) and measuring points.

same, but the intensity increases with downstream distance. Also in the case of 10.0 MPa (test case 4), the spectrum seems to be nearly unchanged (Fig. 18). However, the radiation intensity is 2–3 times stronger compared to the 6.0-MPa case. This tendency seems to be reasonable if we extrapolate the results of Burrows et al.<sup>10</sup> He found that the oxygen/hydrogen flame radiation intensity, especially the OH lines, the  $O_2$ , and the continuum, varied with the pressure as  $p^n$ , where  $n$  varied for the continuum from 3.2 to 2.4 over the pressure range 1.0–3.2 MPa, and for  $O_2$  from 2.6 to 2.0 over the pressure range 1.0–22.7 MPa. The dependency of line intensities on mixture ratio ( $O/F$ ) was small, indicating that the combustion gases were undergoing various degrees of reaction with a wide distribution in gas temperature and composition.

The decreased radiation intensity at position  $x = 70$  mm (Fig. 18) shows that the oxidizer is almost fully depleted. This co-

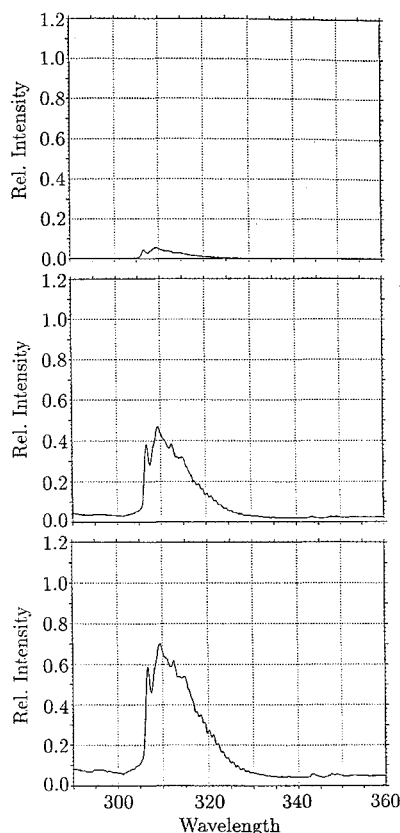


Fig. 17 Spectra of oxygen/hydrogen flame, uv range 290–360 nm, from top to bottom: oxygen jet positions  $x = 10, 40$ , and  $70$  mm, respectively, chamber pressure is  $6.0$  MPa (test case 3).

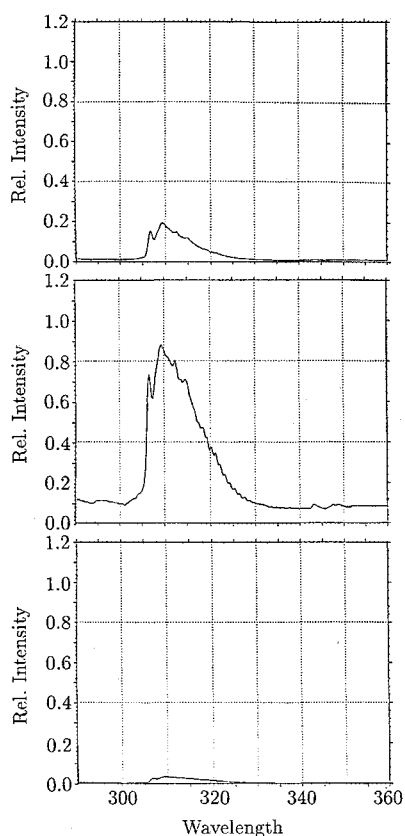


Fig. 18 Spectra of oxygen/hydrogen flame, uv range 290–360 nm, from top to bottom: oxygen jet positions  $x = 10, 40$ , and  $70$  mm, respectively, chamber pressure is  $10.0$  MPa (test case 4).

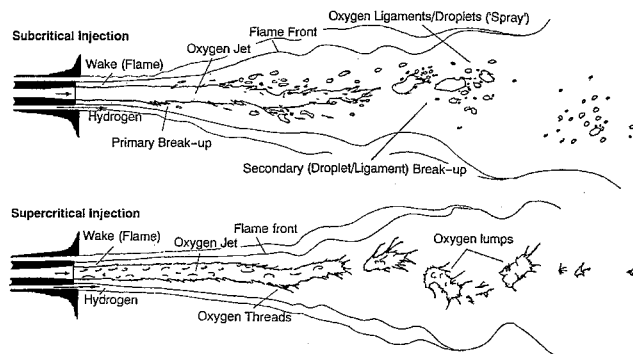


Fig. 19 Schematic of sub- and supercritical injection, respectively.

incides with the spark photographs (Fig. 6) where the end of the LOX jet could be visualized.

### Summary of Results

Results of combustion experiments utilizing liquid oxygen and gaseous hydrogen at chamber pressures between  $1.5$ – $10.0$  MPa have been presented. The phenomena of injection, ignition, and steady-state combustion have been investigated. The spark light photographs demonstrate the dramatic change of the mixing process approaching and exceeding supercritical pressure conditions (Figs. 4–6). In the case of subcritical pressures, i.e., chamber pressures much less than  $5.0$  MPa, the LOX jet is atomized forming a spray comparable to the flow pattern of cold flow atomization before ignition, or as known from cold flow studies. Ligaments are detached from the LOX jet surface, which form round droplets and finally evaporate. At  $1.5$ -MPa chamber pressure (test case 1) secondary break up (droplet vibrational- and bag-type break up) was observed. Because of the rapid vaporization of the droplets in a burning spray, the droplet number density is rather low compared to the cold flow case.

Upon approaching and exceeding supercritical pressure, droplets no longer exist. From the LOX jet core, stringy- or thread-like structures develop and grow, which do not detach, but rapidly dissolve and fade away. At about 50 diameters further downstream, the LOX core breaks up into large LOX lumps, which dissolve in the same manner. Before break up, snake-like nonaxisymmetric oscillations of the jet with an amplitude of a few jet diameters were observed (Fig. 7). Because of the strong convection in the chamber, a hard number of the chamber pressure that demarcates the change of phenomena does not exist. When exceeding  $4.5$ -MPa chamber pressure, no change of flow phenomena could be observed in this study.

Figures 8 and 9 show the flame and the flowfield inside the combustion chamber close to the injector. The results of the spark photography, flame photography, and high-speed cinematography revealed another important mixing phenomenon. The flame always attaches instantaneously after ignition to the LOX post. In the small, but intensive, recirculation zone behind the LOX post, a well-mixed flame with strong radiation forms. The influence of this LOX post wake, which can be tracked at least 15 LOX jet diameters downstream, controls the LOX/GH<sub>2</sub> mixing process, the interface between the LOX and hydrogen propellants is separated by a layer of reacting combustion gases.

The influence of the hydrogen injection temperature, i.e., hydrogen injection density to the mixing process, was found to be less effective than the effect of chamber pressure itself. It seems that the flame tends to separate the propellants. It can be concluded that the injection of LOX and hydrogen and hypergol bipropellants behave much more similarly than previously expected.

Some details of injector design could be clarified, especially the effect of a recessed LOX post. The results of this study led to the hypothesis that in view of combustion instability the advantage of using recessed LOX posts is not the improved atomization performance as known from cold flow tests. During combustion the farfield with and without recess looks the same. Also, in regard to performance, recess has no major effect on it. However, the cup recess region can be regarded as a small and undisturbed combustion chamber that always keeps the propellants ignited and well mixed in an area close to the injector, insensible to disturbances in the chamber.

### Conclusions and Recommendations

The results of this study showed that it was crucial to visualize the injection and mixing process under relevant combustion conditions. On the one hand the effect of the flame on the atomization process could be demonstrated. On the other hand the main mixing processes approaching and exceeding supercritical pressure conditions could be clarified as follows:

1) During ignition and combustion the interface between the propellants is always separated and affected by a layer of hot reacting gas. The flame is attached to the LOX post.

2) As the critical pressure is approached and exceeded, droplets no longer exist. The oxidizer jet surface shows very fine thread- or stringy-like structures that rapidly dissolve. Further downstream, the LOX jet develops nonaxisymmetric snake-like oscillations of growing amplitude until it breaks up; large lumps of oxygen were visualized several tens of jet diameters downstream. This heavy mixing zone is characterized by large-scale turbulence, maximum amplitudes of oxygen jet oscillations, slight widening of the oxygen jet and of the flame, dispersion of the oxygen ligaments or the threads, and strongest combustion radiation. The experimental findings are compiled in a sketch (Fig. 19).

### Modeling

The use of models with the liquid core approach has to be modified to include LOX jet oscillation and break up. Droplet tracking methods to describe the oxidizer or simulations using predefined droplet distribution functions seem to be limited to subcritical injection conditions before ignition. A sophisticated modeling approach has to include submodels for the fine surface phenomena at the oxygen jet, the oxidizer threads, the jet break up, and the dissolution of the large oxidizer lumps in the frame of a turbulent fluid/fluid mixing (shear) flow simulation with chemical reaction.

### Diagnostics

The relevance of shear coaxial injector characterization using droplet distributions is limited to the case of subcritical pressure conditions before ignition, and only for locations very far downstream.

Detailed quantitative measurements of flow and species distribution are needed for model verification. Because of the strong density gradients at high chamber pressures, the use of a laser-optical diagnostic means seems to be limited on principle.

### Injector and Combustion Chamber Design

The experimental results give a lot of instructions for controlled injector design. For example, any change of LOX post tip thickness will sensibly influence the LOX post wake, and thereby control the flameholding mechanism, mixing, and combustion. Absolute chamber pressure plays an important role for the characterization of injector performance.

### Acknowledgments

Funding by the DLR, National Aerospace Laboratory, and STA is gratefully acknowledged. This study was conducted as a joint research project with NAL. We thank our colleagues of the Rocket Combustor Laboratory group, especially H. Sakamoto, M. Sasaki, M. Takahashi, and T. Tomita for support, cooperation, and assistance in conducting the experiments.

### References

- <sup>1</sup>Mayer, W., "Coaxial Atomization of a Round Liquid Jet in a High Speed Gas Stream: A Phenomenological Study," *Experiments in Fluids*, Vol. 16, No. 6, 1994, pp. 401–410.
- <sup>2</sup>Mayer, W., and Krülle, G., "Rocket Engine Coaxial Injector Liquid/Gas Interface Flow Phenomena," *Journal of Propulsion and Power*, Vol. 11, No. 3, 1995, pp. 513–518.
- <sup>3</sup>Puissant, C., Glogowski, M., and Micci, M. M., "Experimental Characterization of Shear Coaxial Injectors Using Liquid/Gaseous Nitrogen," *Proceedings of the 6th ICLASS* (Rouen, France), Begell House Inc., New York, 1994, pp. 672–679.
- <sup>4</sup>Schik, A., and Krülle, G., "Investigation of Supercritical Coaxial Injection in  $H_2/O_2$  Rocket Engines," *Proceedings of the Conference on Propulsive Flows in Space Transportation Systems* (Bordeaux, France), Vol. 1, Centre National d'Etude Spatiales, France, 1995, pp. 118–127.
- <sup>5</sup>Hefner, R. J., and Harrie, D., "Liquid Propellant Rocket Combustion Instability," NASA SP-194, 1972, pp. 451–536.
- <sup>6</sup>Beisler, M. A., Pal, S., Moser, M. D., and Santoro, R. J., "Shear Coaxial Injector Atomization in a LOX/GH2 Propellant Rocket," AIAA Paper 94-2775, June 1994.
- <sup>7</sup>Vogel, A., "Investigations on Atomization of a Coaxial Injected GH2/LOX Jet Under Hot Fire Conditions," *Proceedings of the 6th ICLASS* (Rouen, France), Begell House Inc., New York, 1994, pp. 742–749.
- <sup>8</sup>Mayer, W., and Vogel, A., "Injection and Mixing of Propellants in GH2/LOX Rocket Engines Under Cold Flow and Hot Fire Conditions," *Proceedings of the FEDSM'95, Symposium on Flow Visualization and Image Processing of Multiphase Systems*, American Society of Mechanical Engineers, New York, Aug. 1995.
- <sup>9</sup>Wyett, L., and Reinert, J., "Engine Performance Analysis with Plume Spectrometry," *Threshold*, Rockwell International, Canoga Park, CA, 1992, pp. 45–51.
- <sup>10</sup>Burrows, R., and Povinelli, L., "Emission Spectra from High Pressure Hydrogen-Oxygen Combustion," NASA TN D-1305, July 1962.